arXiv:1607.00962v1 [cond-mat.mes-hall] 4 Jul 2016

Auger recombination of dark excitons in WS_2 and WSe_2 monolayers

Mark Danovich, Viktor Zólyomi, Vladimir I. Fal'ko

National Graphene Institute, University of Manchester, Booth St E, Manchester M13 9PL, UK

Igor L. Aleiner

Physics Department, Columbia University, New York, NY 10027, USA

Abstract. We propose a novel phonon assisted Auger process unique to the electronic band structure of monolayer transition metal dichalcogenides (TMDCs), which dominates the radiative recombination of ground state excitons in Tungsten based TMDCs. Using experimental and DFT computed values for the exciton energies, spin-orbit splittings, optical matrix element, and the Auger matrix elements, we find that the Auger process begins to dominate at carrier densities as low as 10^{9-10} cm^{-2}, thus providing a plausible explanation for the low quantum efficiencies reported for these materials.

E-mail: mark.danovich@postgrad.manchester.ac.uk

Recently, there was an expansive interest in Monolayer transition metal dichalcogenides (TMDCs) due to their potential in optoelectronic applications [1–3]. In contrast to bulk TMDC crystals, the monolayers of $MoS_2, MoSe_2, WS_2$, and WSe_2 are direct band semiconductors. Contrary to $III-V$ semiconductors, in these hexagonal 2D crystals the conduction (c) and valence (v) bands edges are at the K/K' points of the Brillouin zone (BZ) rather than at the Γ-point. Several experiments have alre-ady demonstrated a strong light-matter interaction in these 2D crystals [4].

Potentially practical implementations of these TMDC atomic crystals in optoelectronic devices require high quantum efficiency of the optical process. However, despite the recent progress in improving the quality of 2D TMDCs, the quantum efficiency observed in photoluminescence experiments [5–7] never exceeded 1%. Such systematically low quantum efficiency calls for finding the mechanism responsible for the non-radiative recombination of electron-hole pairs, excitons, or trions.

Here we show that there exists a phonon assisted Auger recombination process illustrated in Fig. 1, which is specific for 2D TMDC semiconductors. By explicit comparison of the phonon assisted radiative recombination rate of ground state excitons in monolayers of WS_2 and WSe_2 with the rate due to the suggested Auger mechanism, we find that the latter starts dominating at electron densities as low as 10^{9-10} cm^{-2}. The specific band structure of 2D TMDCs defies the common wisdom (based on III-V semiconductors studies) that the 2D confinement quenches Auger recombination processes. Namely, electrons from the vicinity of the conduction band (c) edge, can undergo a transition into one of the higher bands (c' in Fig. 1) which is almost in resonance with the exciton annihilation. Both c and c' bands are comprised of d-orbitals of the same metal atom, facilitating the Auger transition.

The electron band structure near the corners of the BZ is described by

$$\hat{H}_0 = \sum_{\nu\sigma\tau} \int d^2\vec{r}\Psi^\dagger_{\nu\sigma\tau}\epsilon_{\nu\sigma\tau}(-i\hbar\nabla)\Psi_{\nu\sigma\tau}, \qquad (1)$$

where $\nu = v, c, c'$, $\sigma = \pm(\uparrow,\downarrow)$, and $\tau = \pm(K, K')$. With reference to the band structure shown in Fig. 1, the relevant spectrum of electrons in the vicinity of the BZ corners can be described using the effective mass approximation as $\epsilon_\nu = E_{\nu\sigma\tau} + \frac{\hbar^2k^2}{2m_\nu}$. Here

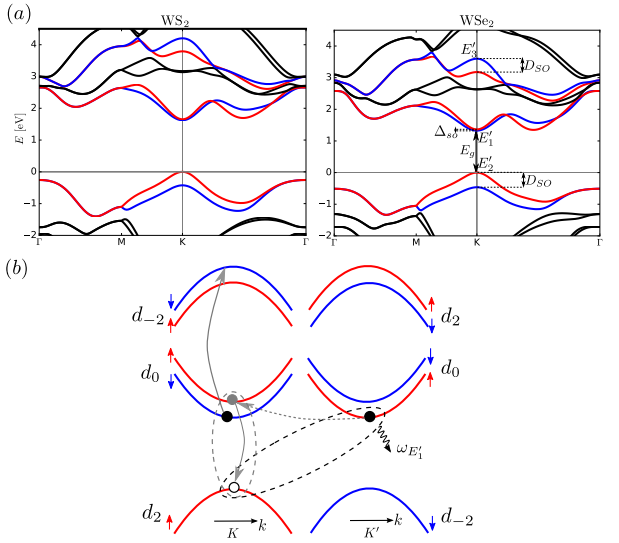

Figure 1. (a) DFT calculated [8] band structure of WS_2 and WSe_2. (b) Sketch of the electronic band structure near the K/K' points, and schematics of the phonon assisted Auger process. The dashed gray line corresponds to the virtual transition.

we count energies from the v band edge and $E_v = -\frac{D_{SO}}{2}(1-\tau\sigma)$, with $m_v < 0$. For the conduction bands we use $E_c = E_g + \frac{\Delta_{SO}}{2}(1+\tau\sigma)$, and $E_{c'} = 2E_g + \Upsilon - \frac{D_{SO}}{2}(1+\tau\sigma)$. Due to mirror plane symmetry (σ_h) of 2D TMDCs, the electron spin projection on to the z-axis normal to the plane σ, is a good quantum number. The signs of spin-orbit splittings in E_c reflect the inverted order of spin-split states in c and v bands specific to Tungsten based TMDCs [9, 10] (in contrast to their Molybdenum counterparts). This results in a ground state exciton/trion which is dark due to spin and momentum conservation constraints [11], requiring emission of K-point phonons for recombination.

To classify suitable options for the radiative and non-radiative transitions in 2D WS_2 and WSe_2, we analyze its symmetry group and write down the corresponding terms in the Hamiltonian. The point group of 2D TMDCs is D_{3h}, which is a direct product group, $C_{3v} \otimes \sigma_h$, where σ_h is the horizontal mirror reflection. The states belonging to the v, c, and c' bands near the K/K'-points are composed of the d_0, d_2 and d_{-2} metal orbitals which posses $z \to -z$ symmetry [10], and therefore belong to the identity irreducible representation (irrep) of σ_h. As a result, we can focus on the point group C_{3v} for the classification of the electronic states into irreps, as well as the classification

Table 1. Character table for the irreducible representations of the extended point group C''_{3v}, and their correspondence to the relevant fermionic and bosonic fields.

C''_{3v}	E	t, t^2	$2C_3$	$9\sigma_v$	$2tC_3$	$2t^2C_3$	
A_1	1	1	1	1	1	1	
A_2	1	1	1	-1	1	1	
E	2	2	-1	0	-1	-1	$(\mathcal{E}_x, \mathcal{E}_y)$
E'_1	2	-1	-1	0	2	-1	Ψ_c
E'_2	2	-1	2	0	-1	-1	Ψ_v
E'_3	2	-1	-1	0	-1	2	$\Psi_{c'}$
D_{xy}	12	0	0	0	-3	-3	phonons
D_z	3	0	0	1	3	0	b

Table 2. Product table for the irreducible representations of the extended point group C''_{3v}.

C''_{3v}	A_1	A_2	E	E'_1	E'_2	E'_3
A_1	A_1	A_2	E	E'_1	E'_2	E'_3
A_2	A_2	A_1	E	E'_1	E'_2	E'_3
E	E	E	$A_1 \oplus A_2 \oplus E$	$E'_2 \oplus E'_3$	$E'_1 \oplus E'_3$	$E'_1 \oplus E'_2$
E'_1	E'_1	E'_1	$E'_2 \oplus E'_3$	$A_1 \oplus A_2 \oplus E'_1$	$E \oplus E'_3$	$E \oplus E'_2$
E'_2	E'_2	E'_2	$E'_1 \oplus E'_3$	$E \oplus E'_3$	$A_1 \oplus A_2 \oplus E'_2$	$E \oplus E'_1$
E'_3	E'_3	E'_3	$E'_1 \oplus E'_2$	$E \oplus E'_2$	$E \oplus E'_1$	$A_1 \oplus A_2 \oplus E'_3$

of phonon modes coupling to the electrons states. Since the states at the K and K'-points are degenerate, it is advantageous to treat them simultaneously. This is achieved by tripling the unit cell, resulting in a three times smaller Brillouin zone in which the K and K' points are folded into the Γ-point [12]. Tripling of the unit cell is achieved by factoring out two translations from the space group of the crystal resulting in the new point group $C''_{3v} = C_{3v} + tC_{3v} + t^2C_{3v}$, where t denotes translation by a lattice vector, and $t^3 = 1$. The character table of the new point group containing 18 elements and 6 irreps is given in Table 1. In the same table we list the electron and photon fields corresponding to the irreps. The decomposition of the direct products of irreps is shown in Table 2.

Using Table 1 one can write down the Hamiltonian for the interaction of the electrons with light [13, 14],

$$H_r = \frac{e\hbar v}{E_g} \sum_{\sigma,\tau} \int d^2\vec{r}\, \Psi^\dagger_{c\sigma\tau} \Psi_{v\sigma\tau} (\mathcal{E}_x + i\tau\mathcal{E}_y) + h.c., \quad (2)$$

where e is the electron charge, v is the velocity originating from the off-diagonal momentum matrix element, and $\vec{\mathcal{E}}$ is the electric field of light. We note that for the excitons, $\Psi^\dagger_c(\vec{r}_1)\Psi_v(\vec{r}_2) \to X^\dagger(\vec{R})\phi(\vec{r}_1 - \vec{r}_2)$, where $\vec{R}$ is the center-of-mass position of the exciton. All possible states of the exciton boson operator X, can be further classified according to the irreps. The dark and bright excitonic states transform according to the direct product representation of the c and v band states $E'_1 \otimes E'_2 = E \oplus E'_3$. The excitons can further be classified according to the spin projection S_z. Due to conservation of spin, the bright state must have $S_z = 0$, which corresponds to the excited state transforming according to the E irrep, and only such a combination enters into Eq. (2). The $(E'_3, S_z = 0)$ states are the intervalley excitons that are dark due to the momentum mismatch. However, these states can radiatively recombine with the help of phonon emission. According to Table 2, this can be provided by phonons from E'_1 and E'_2 irreps. The other exciton doublets, $(E, |S_z| = 1)$ and $(E'_3, |S_z| = 1)$, are absolutely dark due to spin conservation (σ_h reflection changes the sign of the spin projection S_z.)

According to the sign of the spin-orbit splitting in the c band [see text after Eq. (1)], $(E'_3, S_z = 0)$ and $(E, |S_z| = 1)$ are the exciton ground states. Therefore, the decay of these states is the bottleneck for the PL. In this case the PL quantum efficiency is determined by the ratio of the radiative and non-radiative Auger rates.

The Auger process is caused by the electron-electron scattering with momentum transfer of the order of inverse lattice constant, therefore in the effective mass approximation it is described by a contact interaction. Table 1 shows that the only

Table 3. Material parameters used for the rates calculation.

	$\frac{m_c}{m}$ [a]	$\frac{m_v}{m}$ [a]	$\frac{m_{c'}}{m}$	Δ_{SO} [meV]	D_{SO} [eV]	$E_g^{\rm b}$ [eV]	Υ [eV]	$\frac{v}{c}$ [a]	α
WS_2	0.26	−0.35	0.39	30	0.42	2.0	0.6	1.7×10^{-3}	0.5
WSe_2	0.28	−0.36	0.35	38	0.46	1.7	0.6	1.6×10^{-3}	0.6

[a] Ref. [9]
[b] Ref. [14]

combination allowed by symmetry is

$$H_c = \frac{\alpha\hbar^2}{m_{c'}}\sum_{\sigma,\tau}\int d^2\vec{r}\left(\Psi^\dagger_{v\sigma}\Psi^\dagger_{c'-\sigma}\Psi_{c-\sigma}\Psi_{c\sigma}\right)_{\vec{r}\tau} + h.c. \quad (3)$$

Here, α is a dimensionless parameter computed from the matrix element of the Coulomb interaction in the basis of the density functional theory (DFT) wavefunctions (see Table 3). According to Table 2, the initial dark state exciton $(E_3', S_z = 0)$ and the electron (E_1') direct product does not include the final state c' state E_3', making the direct process impossible, hence requiring an extra phonon in the final state. Using Table 2, one finds that this additional phonon in the final state should be the same σ_h symmetric (E_1' or E_2') as involved in the radiative process, allowing the direct comparison of the radiative and Auger rates without relying on the knowledge of the strength of the electron-phonon interaction constants‡. To consider the electron-phonon interaction only on symmetry grounds, we list in Table 1 the representations corresponding to the in-plane D_{xy}, and out of plane D_z modes in the tripled unit cell, which is needed to describe all σ_h symmetric phonon modes in the Γ and K points. From the decomposition $D_{xy} = 2E \oplus E_1' \oplus 2E_2' \oplus E_3'$ and $D_z = A_1 \oplus E_1'$, we conclude that the existence and number of modes needed to facilitate the processes described are protected by symmetry. To mention, in our earlier studies [15] we noticed that the coupling of c band electrons with the homopolar phonon mode A_1 is very strong, which hints that the E_1' mode of D_z, would be the most relevant for the process.

The Hamiltonian describing the E_1' phonon and its interaction with the c band electrons

$$H_{ph} = \hbar\omega\sum_\tau\int d^2\vec{r}\, b^\dagger_\tau(\vec{r})b_\tau(\vec{r}) \quad (4)$$
$$+g\sum_{\sigma,\tau}\int d^2\vec{r}\left(\Psi^\dagger_{c\sigma\tau}\Psi_{c\sigma-\tau}b^\dagger_\tau + h.c.\right),$$

‡ The process involving the emission of an E_2' phonon mode, which couples to the hole, involves the hole scattering into the lower spin-split v band which results in the appearance of the large D_{SO} spin-orbit splitting in the denominator of the rates. Therefore, we neglect the contribution of the E_2' phonon assisted process to the total rates.

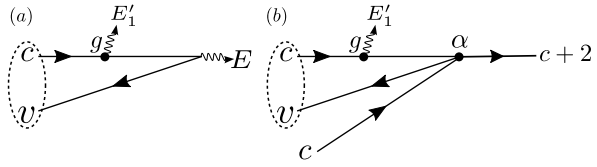

Figure 2. Diagrams for the calculation of the quantum mechanical amplitudes for the (a) phonon assisted radiative process, and (b) phonon assisted Auger process.

where $b(r)$ is the phonon operator in mode E_1' with energy $\hbar\omega$, and g is the coupling coefficient. The radiative (with photon line shifted down by $\hbar\omega$ from the dark exciton energy) and non-radiative rates processes are calculated using the Fermi Golden rule, with the quantum mechanical amplitudes shown in Fig. 3. The rates are given by

$$\frac{1}{\tau_r} = \frac{8E_g}{3\hbar}\frac{e^2}{\hbar c}\left(\frac{v}{c}\right)^2\frac{|\phi(0)|^2g^2}{(\Delta_{SO}+\hbar\omega)^2}, \quad (5)$$

$$\frac{1}{\tau_A} = \frac{E_g}{\hbar}\frac{\hbar^2 n_e}{m_{c'}E_g}\frac{\alpha^2|\phi(0)|^2g^2}{[\Delta_{SO}+\hbar\omega+\frac{m_{c'}}{|m_v|+m_c}\Upsilon]^2}, \quad (6)$$

where n_e is the electron density. Taking the ratio of the two rates we obtain

$$\frac{\tau_r}{\tau_A} = \frac{n_e}{n_e^*}, \quad (7)$$

where the characteristic density is given by

$$n_e^* = \frac{8m_{c'}E_g}{3\hbar^2}\left(\frac{v}{\alpha c}\right)^2\left(\frac{e^2}{\hbar c}\right)\left(1+\frac{\frac{m_{c'}}{|m_v|+m_c}\Upsilon}{\Delta_{SO}+\hbar\omega}\right)^2. \quad (8)$$

We emphasize that the latter equation does not involve the unknown electron-phonon coupling constant. Therefore, we can estimate the values of n_e^* for WS_2 and WSe_2 based on the parameters of these 2D crystals found in DFT and the experimentally known E_g, listed in Table 3:

$$n_e^*(WS_2) \sim 10^{10}\ \text{cm}^{-2},\ n_e^*(WSe_2) \sim 4\times10^9\ \text{cm}^{-2}. \quad (9)$$

These electron concentrations which determine the threshold for efficient photoluminescence are remarkably low. This suggests that the proposed mechanism of Auger recombination dominates over the radiative recombination for all realistic structures.

The authors thank T. Heinz, M. Potemski and A. Tartakovski for discussions. This work was supported by Simons Foundation (IA), ERC Synergy Grant Hetero2D (VF), EC-FET European Graphene Flagship (VZ), EPSRC grant EP/N010345/1 (VF, MD).

[1] Jariwala D, Sangwan V K, Lauhon L J, Marks T J and Hersam M C 2014 *ACS Nano* **8** 1102–1120 URL http://dx.doi.org/10.1021/nn500064s

[2] Wang Q H, Kalantar-Zadeh K, Kis A, Coleman J N and Strano M S 2012 *Nat. Nanotechnol.* **7** 699–712 URL http://dx.doi.org/10.1038/nnano.2012.193

[3] Cao T, Wang G, Han W, Ye H, Zhu C, Shi J, Niu Q, Tan P, Wang E, Liu B and Feng J 2012 *Nat. Commun.* **3** 887 URL http://dx.doi.org/10.1038/ncomms1882

[4] Liu X, Galfsky T, Sun Z, Xia F, Lin E c, Lee Y H, Kéna-Cohen S and Menon V M 2015 *Nat Photon* **9** 30–34 URL http://dx.doi.org/10.1038/nphoton.2014.304

[5] Mak K F, Lee C, Hone J, Shan J and Heinz T F 2010 *Phys. Rev. Lett.* **105**(13) 136805 URL http://link.aps.org/doi/10.1103/PhysRevLett.105.136805

[6] Splendiani A, Sun L, Zhang Y, Li T, Kim J, Chim C Y, Galli G and Wang F 2010 *Nano Letters* **10** 1271–1275 URL http://dx.doi.org/10.1021/nl903868w

[7] Wang H, Zhang C and Rana F 2015 *Nano Letters* **15** 339–345 URL http://dx.doi.org/10.1021/nl503636c

[8] Giannozzi P, Baroni S, Bonini N, Calandra M, Car R, Cavazzoni C, Ceresoli D, Chiarotti G L, Cococcioni M, Dabo I, Dal Corso A, de Gironcoli S, Fabris S, Fratesi G, Gebauer R, Gerstmann U, Gougoussis C, Kokalj A, Lazzeri M, Martin-Samos L, Marzari N, Mauri F, Mazzarello R, Paolini S, Pasquarello A, Paulatto L, Sbraccia C, Scandolo S, Sclauzero G, Seitsonen A P, Smogunov A, Umari P and Wentzcovitch R M 2009 *Journal of Physics: Condensed Matter* **21** 395502 (19pp) URL http://www.quantum-espresso.org

[9] Kormnyos A, Burkard G, Gmitra M, Fabian J, Zolyomi V, Drummond N D and Fal'ko V 2015 *2D Materials* **2** 022001 URL http://stacks.iop.org/2053-1583/2/i=2/a=022001

[10] Liu G B, Xiao D, Yao Y, Xu X and Yao W 2015 *Chem. Soc. Rev.* **44**(9) 2643–2663

[11] Zhang X X, You Y, Zhao S Y F and Heinz T F 2015 *Phys. Rev. Lett.* **115**(25) 257403 URL http://link.aps.org/doi/10.1103/PhysRevLett.115.257403

[12] Basko D M 2008 *Phys. Rev. B* **78**(12) 125418 URL http://link.aps.org/doi/10.1103/PhysRevB.78.125418

[13] Esser A, Runge E, Zimmermann R and Langbein W 2000 *Phys. Rev. B* **62**(12) 8232–8239 URL http://link.aps.org/doi/10.1103/PhysRevB.62.8232

[14] Palummo M, Bernardi M and Grossman J C 2015 *Nano Letters* **15** 2794–2800

[15] Danovich M, Aleiner I, Drummond N D and Fal'ko V 2015 Fast relaxation of photo-excited carriers in 2d transition metal dichalcogenides (*Preprint* arXiv:1510.06288)